High Performance Linear-Quadratic and H-Infinity Designs for a "Supermaneuverable" Aircraft

Petros Voulgaris* and Lena Valavani†
Massachusetts Institute of Technology, Cambridge, Massachusetts

Recent efforts by the NASA Langley Research Center have focused on expanding the flight envelope of the F/A-18 aircraft. Of particular concern has been the low speed, high angle-of-attack regime over which the conventional aerodynamic controls of the F/A-18 lose their effectiveness. To address this problem, the F18 high alpha research vehicle (HARV) was developed. This aircraft is essentially a modified F/A-18 that possesses thrust vectoring capabilities and hence increased maneuverability in this flight regime. In this paper, the linear-quadratic-Gaussian/loop-transfer-recovery and H_∞ design methodologies are used to design high-performance controllers for the HARV at an operating point within the expanded envelope. In addition, this paper shows how the control redundancy of the HARV can be used to maintain nominal performance, as well as nominal stability, in situations where failures occur.

Nomenclature

$K(s)$ = compensator
$M(s)$ = finite dimensional LTI system
q = perturbation in pitch rate, rad/s
u = control input vector
V_T = perturbation in true airspeed, ft/s
w = exogenous input vector (commands, disturbances, sensor noise, etc.)
y = measurement vector
z = output (any signal of interest: weighted errors, controls, etc.)
α = perturbation in angle of attack, rad
δ_T = perturbation in throttle position, deg
δ_{as} = perturbation in symmetric aileron deflection, deg
δ_{ss} = perturbation in symmetric stabilator deflection, deg
δ_{les} = perturbation in symmetric leading edge flap deflection, deg
δ_{tes} = perturbation in symmetric trailing edge flap deflection, deg
δ_{tvs} = perturbation in symmetric thrust vectoring vane deflection, deg
θ = perturbation in pitch angle, rad

Introduction

DURING the past few years, research efforts at NASA Langley Research Center have been directed toward enhancing the agility of military aircraft over an expanded flight envelope. This expanded envelope includes the low speed, high angle-of-attack regime over which dynamic pressure is low and conventional aerodynamic controls lose their effectiveness.

Current efforts have focused on a modified version of the Navy's F/A-18 fighter aircraft referred to as the "supermaneuverable" high alpha research vehicle (HARV). This vehicle is referred to as supermaneuverable because, in addition to possessing the conventional aerodynamic controls of the F/A-18, it possesses thrust vectoring vanes, which allow moments to be generated effectively even under low speed, high angle-of-attack combat scenarios. In particular, the control elements of the HARV consist of the following: 1) a large span, single slotted trailing-edge flap capable of 45-deg deflection in the landing configuration but doubling as a differential flaperon with ±8 deg deflection in the up-and-away maneuvering configuration; 2) single slotted, drooped ailerons for takeoff and landing, with ±25 deg deflection for up-and-away conditions; 3) leading-edge flaps, which are scheduled with angle of attack and Mach number to a maximum of 34 deg down. In addition, they are used differentially ±3 deg for roll augmentation; 4) twin rudders, which are used for the normal purposes of directional control and roll coordination but that are used also for enhancement of longitudinal stability and control in the takeoff and landing configurations; and 5) an all-movable stabilator with differential deflection for roll.

Apart from the aerodynamic control surfaces, the vehicle includes the following propulsive control elements: throttle position, which regulates the thrust delivered by the engine, and a thrust vectoring vane system, which regulates the angle at which the thrust is applied on the aircraft.

As already discussed, the HARV possesses many control inputs that can be used to maneuver the aircraft. The coordination of these controls in time, in order to achieve prescribed maneuvers, is a challenging multivariable control problem. It becomes especially challenging at very low speed, high angle-of-attack operating points where the aircraft becomes unstable. Because of this, controlling the vehicle over the expanded envelope is a nontrivial task.

In addressing the preceding highly multivariable control problem, single-input/single-output (SISO) classical ideas become difficult, if not impossible, to use. Consequently, direct multivariable procedures are more suitable.

The linear-quadratic-Gaussian/loop-transfer-recovery (LQG/LTR) methodology as developed by Athans,[1] Stein and Athans,[2] and Doyle and Stein[6] has proven itself an extremely valuable tool for control engineers developing multivariable controllers. The H_∞ design methodology, especially after recent results by Doyle et al.,[14] has also demonstrated great potential as a multivariable design tool. However, unlike the LQG/LTR design methodology, not many multivariable examples of H_∞ designs have appeared in the literature.

In this paper, we use the LQG/LTR and H_∞ design methodologies to design high-performance, multi-input/multi-output (MIMO) controllers for the HARV at an operating point within the high "alpha" regime. In addition, we look at how the control redundancy of the HARV can be used to maintain nominal performance, as well as nominal stability, in situations where failures occur.

Received Nov. 8, 1988; revision received July 24, 1989.

*Graduate Student, Department of Aeronautics and Astronautics.
†Associate Professor, Department of Aeronautics and Astronautics. Associate Fellow AIAA.

Formulation and Analysis of Linear Model of the HARV

The equations describing the motion of an aircraft subject to aerodynamic propulsive and gravitational forces are highly nonlinear functions of many variables.[10] However, linearization of these complicated equations around an operating point provides excellent representation of the motion of the aircraft about that specific trim point. The linearization of the nonlinear equations of motion is usually accomplished by expanding these equations into a Taylor's series about the equilibrium point of interest, while neglecting higher than the first-order terms.

Variable Definitions and State Space Model

An advantage of the linearized model is that the longitudinal and lateral-directional dynamics can be practically decoupled. In this paper only the longitudinal behavior of the aircraft is studied. The linear model describing the longitudinal dynamics of the F18/HARV consists of four states and six control inputs and is of the form

$$\dot{x}(t) = Ax(t) + Bu(t), \qquad A \in R^{4\times 4}, \qquad B \in R^{4\times 6} \tag{1}$$

where

$$x(t) = [V_T\ \alpha\ q\ \theta]^T$$

$$u(t) = [\delta_{tvs}\ \delta_{as}\ \delta_{ss}\ \delta_{les}\ \delta_{tes}\ \delta_T]^T$$

By a symmetric input, we mean the sum of the left and right components (if any) of a particular control element.

In this paper we address a "hard" operating condition at a high angle of attack in the low-speed regime of the flight envelope. In particular, this point represents horizontal flight at an altitude of 15,000 ft with Mach number $M = 0.24$, airspeed $V_T = 238.7$ ft/s, angle of attack $\alpha = 25$ deg, and pitch angle $\theta = 25$ deg. The trim value of the path angle ($\gamma = \theta - \alpha$) is $\gamma = 0$ deg, and the trim pitch rate is $q = 0$ deg/s. In situations like this, the role of thrust vectoring is expected to be important. Parameter values are given in the Appendix.

Selection of Outputs to be Controlled

For fighter aircraft, three longitudinal precision control modes are of major importance.[12] These are the vertical translation, pitch pointing, and direct lift modes. In the vertical translation mode, the flight-path angle γ ($= \theta - \alpha$) is changed and the pitch angle θ is maintained constant. The pitch pointing mode consists of a change in pitch angle θ whereas the flight-path angle γ is kept constant. Finally, in the direct lift mode, both the flight-path angle γ and pitch angle θ change in such a way that the angle of attack α is maintained constant.

Examining the structure of the linear model, as shown in the Appendix, one can see that the input matrix B has rank three. This implies that, in principle, the maximum number of variables that can be controlled independently is three. Furthermore, for the pilot to execute successfully the longitudinal maneuvers previously discussed, he should be able at least to control independently the flight-path angle γ as well as the pitch angle θ. Also, independent and simultaneous control of the airspeed V_T would offer the pilot a great deal of flexibility. For these reasons the outputs to be controlled were chosen as follows:

$$y = \begin{bmatrix} \text{true airspeed } V_T \\ \text{flight path angle } \gamma \\ \text{pitch angle } \theta \end{bmatrix} \tag{2}$$

In this paper, it was assumed that the variables in Eq. (2) are measurable and can be used to generate control signals.

Scaling of Linear Model

Scaling of the variables plays a very important role in multivariable control design.[1] By scaling, the physical units can be eliminated and their interactions are easier to compare and understand. For example, comparing 1-ft/s deviation from trim airspeed with a 1-rad deviation from trim angle of attack does not make a lot of sense from a practical point of view. In fact, one might argue that these deviations are "not comparable."

What does make sense, however, is to compare deviations normalized by scale factors such that a 1-unit deviation from trim airspeed would be of "equal importance" as a 1-unit deviation from trim angle of attack. Having a knowledge of the system (sizes, physical quantities involved, trim conditions, etc.) is helpful, since one can establish a relative importance type of scaling.

As a first step, scaling was performed to convert radians to degrees. Then, based on our physical understanding, the relative importance scaling was decided as shown in Table 1.

With the scaling of variables as shown in Table 1, a 1-deg deviation from trim of path-angle γ is equally important with a 1-deg deviation from trim of pitch-angle θ and 8-ft/s deviation in trim speed V_T. The scaling of the controls was done using the saturation levels. In particular, refer to Table 2.

Control Redundancy of the HARV

As stated, the rank of the input matrix B is equal to three. Therefore, the question to be answered is how to select three of the six available control inputs, or three independent combinations of control inputs that will be used to design the compensator.

One approach would be to select the three that would be expected to perform the best to the demands of the specifications, based on the physical intuition and knowledge of the system. Another way would be to use steady-state (dc) analysis to decide which controls most affect the outputs at steady state. One more option is the so-called "relative control effectiveness technique."[11]

All of the aforementioned methods, however, lack flexibility since the freedom offered by the redundancy of the controls is not used. To be more clear, in the preceding methods, the combinations of the controls are prespecified. If, however, for some reason a certain control cannot operate (e.g., actuator failure), then the need for redesign of the compensator is essential. The approach used in this paper overcomes the shortcomings of the preceding methods by taking full advantage of the redundancy in control inputs. This is described in what follows.

Considering the state space description of the scaled model

$$\dot{x}(t) = Ax(t) + Bu(t) \tag{3a}$$

$$y(t) = Cx(t) \tag{3b}$$

Table 1 Scaling of the variables

Variable	Scaling factor
V_T	1/8 ft/s
γ	1/1 deg
θ	1/1 deg

Table 2 Scaling of the controls

Input	Scaling factor
δ_{tvs}	1/(25 + 25) deg
δ_{as}	1/(25 + 25) deg
δ_{ss}	1/(17 + 17) deg
δ_{les}	1/(1 + 1) deg
δ_{tes}	1/(30 + 30) deg
δ_T	1/27 deg

and taking into account that rank $(B)=3$, it is evident that the term $Bu(t)$ with $B\epsilon R^{4\times 6}$, $u(t)\ \epsilon R^{6\times 1}$ can be equivalently replaced by $B_v\ v(t)$ with B_v any matrix $\epsilon R^{4\times 3}$ such that the space spanned by the columns of B_v is identical to the space spanned by the columns of B and $v(t)$ any vector $\epsilon R^{3\times 1}$. The input $v(t)$ is a fictitious one and, therefore, is called pseudocontrol. Taking into account the specific structure of B since

$$B=\begin{bmatrix} B_1 \\ -0_{1\times 6}- \end{bmatrix} \tag{4}$$

with rank $(B_1)=3$, it is easy to see that a legitimate B_v is the following:

$$B_v=\begin{bmatrix} I_{3\times 3} \\ 0_{1\times 3} \end{bmatrix} \tag{5}$$

Thus, the state space description of the "pseudosystem" when the fictitious input vector $v(t)$ is used is

$$\dot{x}(t)=Ax(t)+B_v v(t) \tag{6a}$$

$$y(t)=Cx(t) \tag{6b}$$

with B_v given by Eq. (5).

Clearly, this system is a square system (number of inputs = number of outputs) and a square compensator based on the pseudocontrols $v(t)$ can be designed.

Given a controller design based on the pseudosystem, one can distribute the pseudosignal $v(t)$ to the actual control $u(t)$ in an "optimal" way subject to $Bu(t)=B_v v(t)$. In view of Eqs. (4) and (5), this constraint can be replaced as

$$B_1 u(t)=v(t) \tag{7}$$

The control distribution optimization problem posed in this paper is

Minimize

$$J=[u^T(t)W(t)u(t)] \tag{8}$$

where $u(t)\epsilon R^{6\times 1}$, subject to $B_1u(t)=v(t)$ with $W(t)=W^T(t)$ any positive definite weighting matrix.

Thus, the pseudocontrol $v(t)$ is distributed in such a way that the weighted "energy" of the actual control input $u(t)$ is minimized. The aforementioned optimization problem has an explicit solution that can be found using several techniques (for example, Lagrange multipliers is an easy way).

The optimal $u(t)$ is given by

$$u(t)=T(t)v(t) \tag{9}$$

with

$$T(t)=\{W^{-1}(t)B_1^T[B_1W^{-1}(t)B_1^T]\} \tag{10}$$

The transformation $T(t)$ is simply a right inverse of B_1. The benefits of using the method described so far in this section come from the fact that there is a lot of freedom to distribute the pseudocontrols to the actual ones once the design based on the pseudosystem is completed. For example, if for some reason certain controls cannot be fully used and one needs to maintain the same performance in terms of response to commands, then one simply has to change the distribution matrix T by heavily weighting these controls.

A point to notice here is that the weighting matrix $W(t)$ can be a continuous function of time, which allows continuous adjustments of the weights on each control input.

Another way of distributing the pseudocontrols is implied by the following optimization problem:

Minimize

$$\{\max(|u_1|, |u_2|,..., |u_6|)\}$$

with $u(t)\epsilon R^{6\times 1}$ subject to $B_1u(t)=v(t)$.

This problem is a purely linear programming problem and its solution cannot be given with a simple explicit formula as in the previous case. However, the solution can be obtained easily using standard linear programming algorithms (e.g., Simplex method). In this optimization problem, the magnitude of the controls is minimized, and thus saturation is avoided to the extent possible.

Pseudosystem Characteristics

For reasons discussed in the preceding section, the controller design will be based on the so-called pseudosystem in which the term $Bu(t)$ is replaced by $B_v v(t)=[I_{3\times 3}\ 0_{3\times 1}]^T v(t)$ where $v(t)$ is the pseudocontrol input. The block diagram representation of the pseudosystem is shown in Fig. 1.

The transfer function matrix from v to y is $G_v(s)=C(sI-A)^{-1}B_v$. The poles and zeros of the pseudosystem are

Poles: $0.0188\pm 0.1280j$ ("phugoid" unstable)
-0.2481 ± 0.3585 ("short period" stable)

Zeros: None

The singular value plot of $G_v(j\omega)$ for the frequency range 0.001–100 rad/s is shown in Fig. 2.

Compensator Design

This section applies the LQG/LTR design methodology to the scaled linear model previously discussed. The H_∞ design methodology is then applied. Finally, comparisons are made and fundamental tradeoffs are described.

Design Specifications

The standard control system configuration is depicted in Fig. 3a. We have to design a controller $K_o(s)$ for the linear model of the aircraft $G_o(s)$ at the selected operating point that will perform certain tasks discussed in the sequel. It is assumed that the actuator dynamics are fast enough so that they can be omitted. As mentioned before, the design will be based on the pseudosystem $G_v(s)$, meaning that a compensator $K_v(s)$ generating the pseudosignal $v(t)$ will be found (Fig. 3b). Then, the "logic" T for distributing the pseudocontrol $v(t)$ to the actual control input $u(t)$ will be incorporated to the compensator structure.

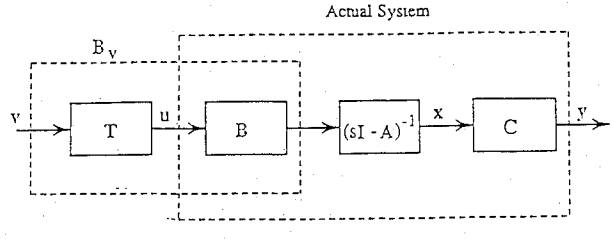

Fig. 1 Pseudosystem $G_v(s)$.

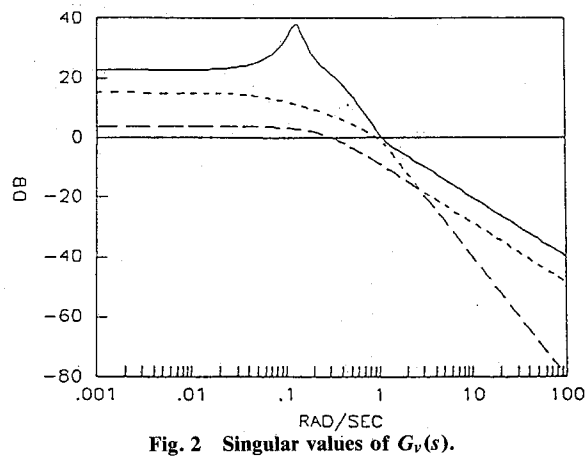

Fig. 2 Singular values of $G_v(s)$.

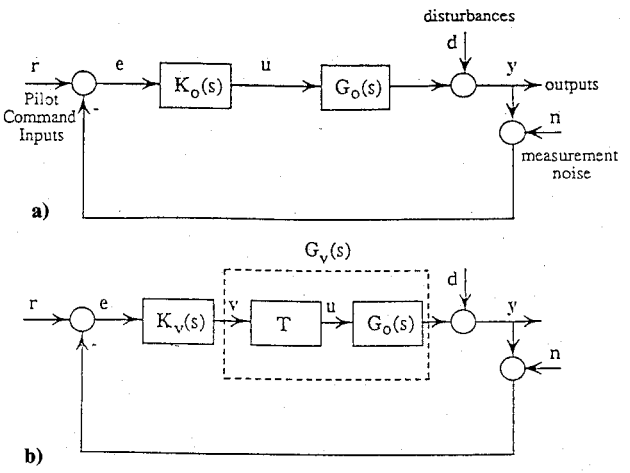

Fig. 3 Control system configuration: a) actual system $G_o(s)$ and b) pseudosystem $G_v(s)$.

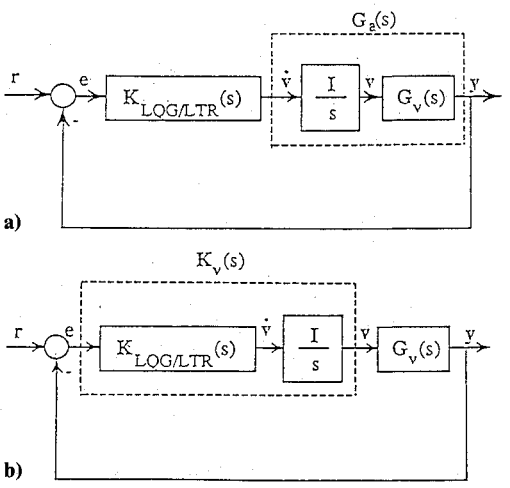

Fig. 4 Augmentation with integrators.

From our discussions with NASA, the following requirements on the compensator were set: 1) nominal stability, 2) performance, and 3) stability robustness. The steady-state error e to low-frequency ($\omega<0.1$ rad/s) sinusoidal commands r or disturbances d should be "small." In particular, note the following performance specifications:

2a) $\|e\|_2 \le 0.1$ for $\omega<0.1$ rad/s whenever $\|r\|_2 \le 1$ or $\|d\|_2 \le 1$.

2b) Zero steady-state error to constant commands or disturbances in all directions.

The system should be fast but excessive control action must be avoided. In particular, the system should track the step commands in Table 3, respecting the magnitude limits as well as the rate limits in the table. The system should be able to reject high-frequency measurement noise n. In particular,

2c) $\|e\|_2 \le 0.1$ for $\omega>20$ rad/s whenever $\|n\|_2 \le 1$.

The system should remain stable in the presence of low-frequency uncertainty and high-frequency unmodeled dynamics. In particular, the following stability robustness specifications should be fulfilled:

3a) Multivariable downward gain margin at the plant output $GM\downarrow \le -4.1$ dB; multivariable upward gain margin at the plant output $GM\uparrow \ge 8.0$ dB; and multivariable phase margin at the plant output $|PM| \ge 35$ deg.

3b) Stability in the presence of multiplicative error $\Delta(s)$ reflected at the plant output that is bounded by $\delta(\omega)=0.1\omega$ for all ω.

The requirements posed previously can be reinterpreted as follows. Performance specifications 2a and 2b simply impose constraints on the sensitivity transfer function $S(s)=[I+G_v(s)K_v(s)]^{-1}$. Namely,

$$\sigma_{\max}[S(j\omega)] \le -20 \text{ dB} \qquad \text{for } \omega \le 0.1 \text{ rad/s}$$

$$\sigma_{\max}[S(j\omega)] \to 0 \qquad \text{as } \omega \to 0$$

Or translating, into the loop-transfer function $G_v(s)K_v(s)$ shapes, since usually for small ω,

$$\sigma_{\min}[G_v(j\omega)K_v(j\omega)] \approx \{\sigma_{\max}[S(j\omega)]\}^{-1}$$

$$\sigma_{\min}[G_v(j\omega)K_v(j\omega) \ge 20 \text{ dB} \qquad \text{for } \omega \le 0.1 \text{ rad/s}$$

$$\sigma_{\min}[G_v(j\omega)K_v(j\omega)] \to \infty \qquad \text{as } \omega \to 0$$

Requirement 2b, along with Table 3, shows the bandwidth constraints of the system and, together with requirement 3a, establishes a tradeoff between response speed, phase and gain margins, and saturation magnitude and rate limits. Specifically, the stability robustness requirement 3a is met if the following condition on

$$\|S(s)\|_\infty = \sup\{\sigma_{\max}[S(j\omega)]\}$$

Table 3 Performance step commands and rate limits

Step commands	
Vertical translation	$r_1 = [0\ 1\ 0]^T$
Pitch pointing	$r_2 = [0\ 0\ 1]^T$
Direct lift	$r_3 = [0\ 1\ 1]^T$
Rate limits	
Thrust vectoring	60 deg/s
Aileron	100 deg/s
Stabilator	60 deg/s
Leading-edge flap	20 deg/s
Trailing-edge flap	60 deg/s
Throttle	30 deg/s

is true:

$$\|S(s)\|_\infty \le 1.66 \approx 4.4 \text{ dB}$$

This sufficient condition results from the following well-known facts[5,7]:

$$GM\downarrow \le \frac{k}{k+1}$$

$$GM\uparrow \ge \frac{k}{k-1}$$

$$|PM| \ge 2 \sin^{-1}(1/2k)$$

where $k=\|S(s)\|_\infty$. Clearly, by minimizing k, we obtain good gain and phase margin properties.

Finally, specifications 2c and 3b also impose constraints on the bandwidth of the system and on the rolloff at high frequencies. Specifically, performance specification 2c requires that

$$\sigma_{\max}[C(j\omega)] \le -20 \text{ dB} \qquad \text{for } \omega > 20 \text{ rad/s}$$

where $C(s)=[I+G_v(s)K_v(s)]^{-1}G_v(s)K_v(s)$ is the closed-loop transfer function. For requirement 3b it is sufficient, resulting from well-known facts on the issue of stability robustness,[4,5] that

$$\sigma_{\max}[C(j\omega)]\ \delta(\omega) < 1 \qquad \text{for all } \omega$$

or, since

$$\sigma_{\max}[G_v(j\omega)K_v(j\omega)] \approx \sigma_{\max}[C(j\omega)]$$

for large enough ω, the preceding constraint can be restated as

$$\sigma_{\max}[G_v(j\omega)K_v(j\omega)] < 10/\omega \qquad \text{for all } \omega$$

Application of the LQG/LTR Design Methodology to the HARV

Since performance specification 2b asks for zero steady-state error to constant commands or disturbances and $G_v(s)$ does not possess any poles at the origin, an integrator is needed for each channel without any feedback around it. Thus, we have to augment $G_v(s)$ by adding integrators in each input channel (Fig. 4a). Then we will proceed to design the LQG/LTR compensator $K_{\text{LQG/LTR}}(s)$ using the augmented system (design plant)

$$G_a(s) = C_a(sI - A_a)^{-1}B_a = G_v(s)I/s$$

that meets the specifications previously posed. Finally, we will absorb the integrators in the LQG/LTR compensator (Fig. 4b) and form the "actual" compensator $K_v(s)$. The detailed procedure can be found in Ref. 13. The target loop of the LQG/LTR methodology, designed with a matching-at-all-frequencies technique,[1] was sufficiently recovered by the transfer function $G_a(s)K_{\text{LQG/LTR}}(s)$ so that the specifications are met. The resulting singular values

$$\sigma_i[G_a(j\omega)K_{\text{LQG/LTR}}(j\omega)]$$
$$\sigma_i[(I + G_a(j\omega)K_{\text{LQG/LTR}}(j\omega))^{-1}]$$

of the loop and of the sensitivity transfer function are shown in Figs. 5 and 6, respectively.

As can be verified from these plots, all of the specifications in the frequency domain are met. The loop crossover is approximately at 2 rad/s and 1 rad/s for the maximum and minimum singular values, respectively, which implies that the settling times should range from approximately $3(1/2) = 1.5$ s up to $3(1/1) = 3$ s.

The stability margins can be inferred from the sensitivity singular values by evaluating $\|S(s)\|_\infty$. By inspection $\|S(s)\|_\infty \approx 4$ dB, which implies that

$$GM\downarrow \leq 0.61 = -4.29 \text{ dB}, \quad GM\uparrow \geq 2.7 = 8.66 \text{ dB}$$
$$|PM| \geq 36.8 \text{ deg}$$

The poles and zeros of the augmented system $G_a(s)$, LQG/LTR compensator $K_{\text{LQG/LTR}}(s)$, and closed loop system $C(s)$ are given in the Appendix.

The resulting (scaled) output response to the direct lift of 1 deg in γ and θ step command $r_3 = [0\ 1\ 1]^T$ is shown in Fig. 7. Figure 8 illustrates what the actual (scaled) inputs should be. The actual control inputs are obtained by distributing the pseudocontrols v so that the quadratic cost $J = u^T W u$ is minimized, with $W = \text{diag}(1, 1, 1, 1, 5.2, 1)$. As it can be verified, the output tracks the reference input with zero steady-state error, negligible overshoots, and with settling time in the range from 1.5 to 3 s. Both saturation magnitude and rate limits are respected. The responses to the vertical translation and pitch pointing reference commands can be found in Ref. 13.

For larger step commands, the controls, depending on the direction of the reference input, may saturate. Saturation can cause instability. A partial solution to the problem is achieved by presmoothing the reference inputs r (something that is always done) by passing them through smoothing filters before entering the feedback loop. Doing so removes unwanted frequencies from the reference commands. Obviously, this "extra baggage" does not alter the stability and performance characteristics of the feedback loop design since the filter is out of the feedback loop. This solution is partial because one cannot introduce shaping filters to presmooth disturbances from nature. However, a recently developed methodology[8] provides a very intelligent way to handle saturating nonlinearities that guarantees stability and degrades the performance minimally. Therefore, saturation seems not to be a problem any more as long as the system one is dealing with is linear.

Application of the H_∞ Methodology to the HARV

The general interconnection structure of a feedback system can be represented as in Fig. 9. The objective in the H_∞ methodology[3] is to find a stabilizing $K(s)$ such that the infinity

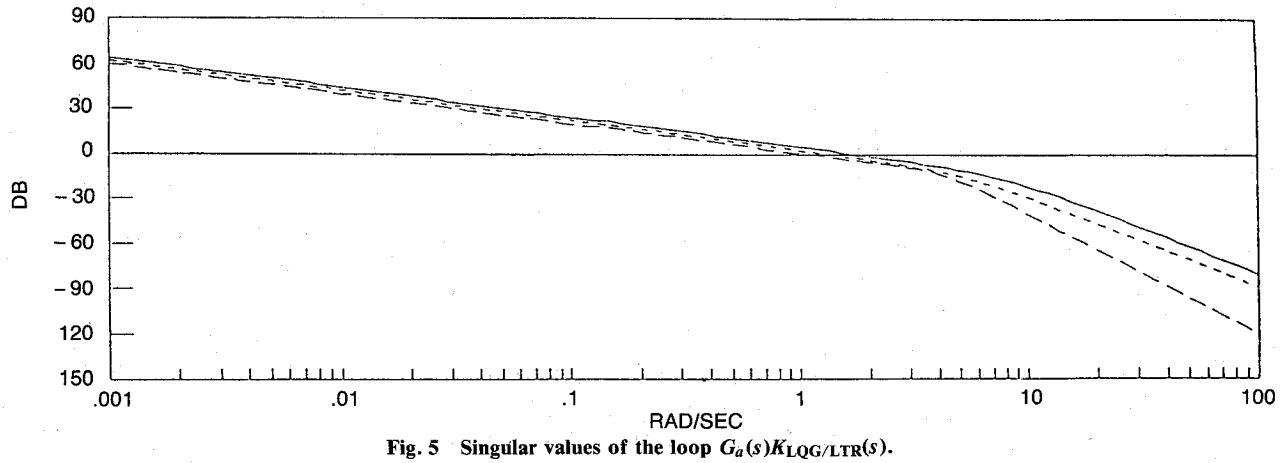

Fig. 5 Singular values of the loop $G_a(s)K_{\text{LQG/LTR}}(s)$.

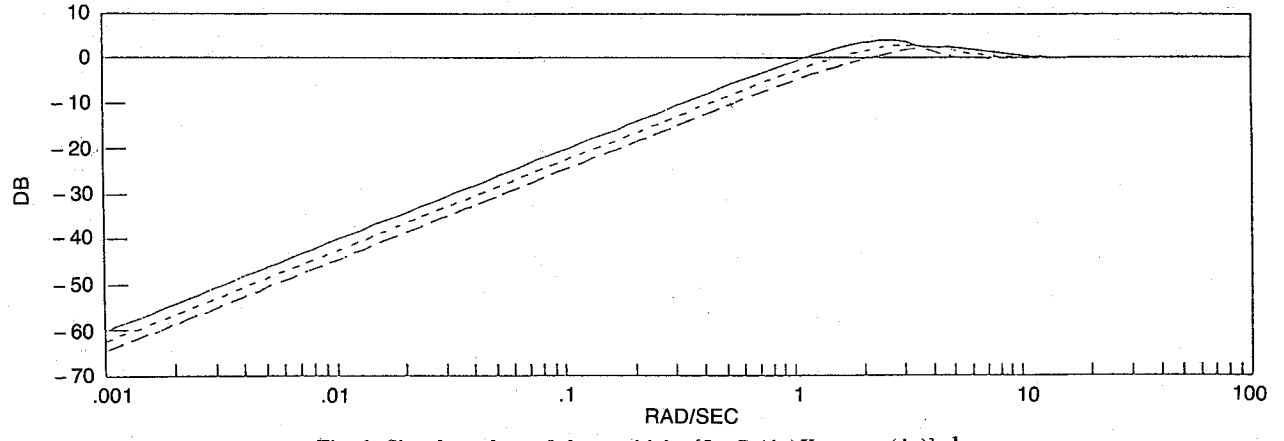

Fig. 6 Singular values of the sensitivity $[I + G_a(j\omega)K_{\text{LQG/LTR}}(j\omega)]^{-1}$.

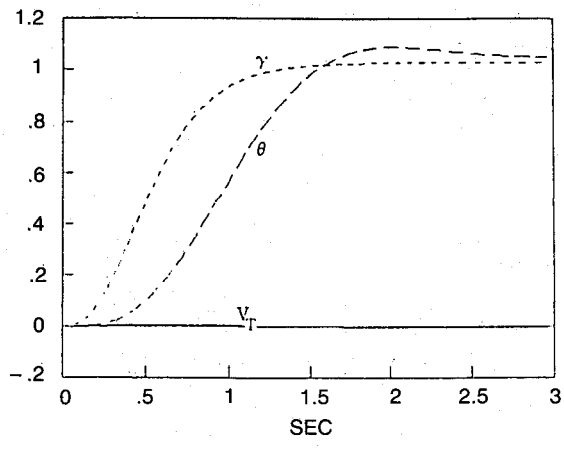

Fig. 7 Output response to r_3.

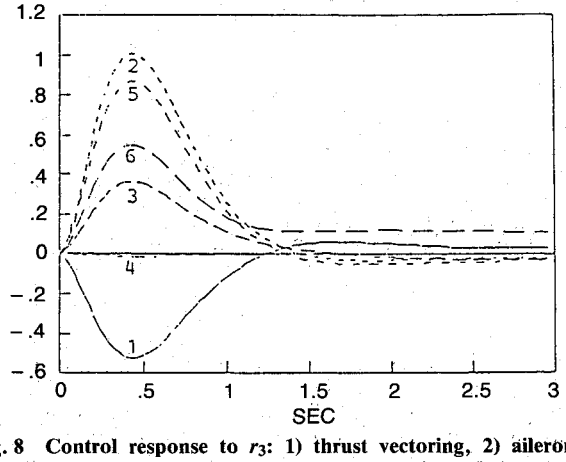

Fig. 8 Control response to r_3: 1) thrust vectoring, 2) aileron, 3) stabilator, 4) leading-edge flap, 5) trailing-edge flap, 6) throttle.

norm $\|H_{zw}(s)\|_\infty$ of the transfer function $H_{zw}(s)$ from w to z is minimized. This can be interpreted in the time domain as minimizing the worst-case energy of the output $z(\|z\|_{L_2})$ when the energy of the input $w(\|w\|_{L_2})$ is bounded. Viewing it in the frequency domain, this minimization implies that the worst-case, steady-state amplitude of the output $z(\|z\|_2)$ is minimized when the input w is a bounded amplitude sinusoid.

In general, the solution of the H_∞ problem cannot be computed directly. However, an iterative scheme, the so-called γ iteration, can be used to find solutions arbitrarily close to the optimal. In particular, this iterative approach consists of finding stabilizing compensators that guarantee

$$\|H_{zw}(s)\|_\infty < \gamma \tag{11}$$

with

$$\gamma > \gamma_{\text{opt}} = \min_{\text{stabilizing } K(s)} (\|H_{zw}(s)\|_\infty) \tag{12}$$

Recent results in the area of H_∞ synthesis by Doyle et al.[14] provide a convenient method to solve the preceding problem by essentially solving two Riccati equations.

The specifications can be used to condition the outputs (and/or inputs) with (stable) weights that are absorbed in the general system $M(s)$. The selection of weights is one of the most important steps in the H_∞ methodology. They are used to emphasize one frequency range over another. It must be kept in mind that the selection of the weights reflects engineering judgment and, thus, a poor selection of these weights may result in poor designs. For example, posing a heavy penalty on the sensitivity $S(s)$ and on the complementary sensitivity $C(s)$ in the same frequency region does not make a lot of sense since $C(s)+S(s)=I$. It should also be noted that the complexity of the compensator, namely its order, is equal to the sum of the orders of the plant, the weights, and a free parameter $Q(s)$

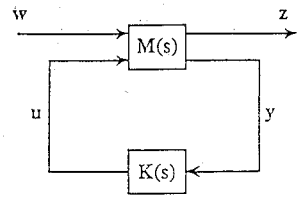

Fig. 9 General framework.

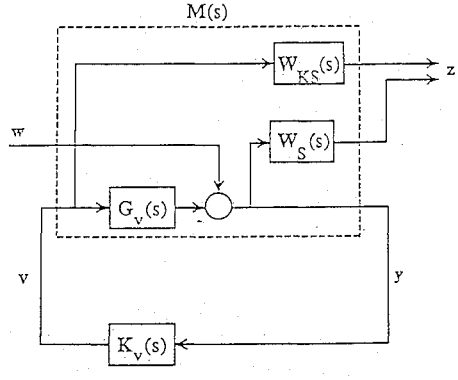

Fig. 10 Framework for the H_∞ compensator design for the pseudosystem.

(resulting from the nonuniqueness of solutions to the H_∞ problem). Therefore high order weights will result in a high order compensator.

In this design the output z is considered as the weighted error signal e and the weighted pseudocontrol v (see Fig. 10). By minimizing $\|H_{zw}(s)\|_\infty$, we minimize

$$\|W_S(s)e(s)\|_{L_2}^2 + \|W_{KS}(s)v(s)\|_{L_2}^2$$

which represents a tradeoff between bandwidth and control action.

Since the specifications ask for zero steady-state error to constant commands and disturbances, the weight $W_S(s)$ should be large at low frequencies. [In fact, $W_S(s)\to\infty$ as $s\to 0$.] The robustness and noise attenuation specifications require that $\sigma_{\max}[S(j\omega)]\approx 1$ for large ω so that $\sigma_{\max}[C(j\omega)]$ rolls off. If the (pseudo) control v is not weighted enough, then the resulting loop tends to have high bandwidth and, thus, the resulting control action is excessive. Consequently, sufficient penalties should be imposed on the control signal v. In particular, the weighting should be heavier as frequency increases so that $K_v(s)S(s)$ would be forced to roll off; thus, extremely fast control action would be prevented. If $K_v(s)S(s)$ is not forced to roll off, then the control action would be more impulsive.

Having these in mind the following (diagonal) weights are selected:

$$W_S(s) = \frac{s+3}{(s+0.0001)(s/1000+1)} I_{3\times 3}$$

$$W_{KS}(s) = \frac{1}{7}\frac{(s/4+1)}{(s/1000+1)} I_{3\times 3}$$

Due to some (mild) strict properness requirements of the Doyle et al. method, a high frequency pole in $W_S(s)$ at $s=-1000$ was inserted. The zero at $s=-3$ indicates the desired bandwidth, whereas the pole at $s=-0.0001$ represents a sufficiently good approximation of a pole at the origin (since the weights are required to be stable) so that the zero steady-state requirement is met. The weighting on the control $W_{KS}(s)$ was adjusted so that the saturation levels were preserved for the commands considered before. The fast pole at $s=-1000$ was inserted to make $W_{KS}(s)$ proper.

Performing the steps of the Doyle et al. algorithm, a compensator $K_v(s)$ that stabilizes the system and guarantees $\|H_{zw}(s)\|_\infty \leq 2.525$ was obtained (the minimum value γ_{opt} of $\|H_{zw}(s)\|_\infty$ over all stabilizing controllers $K_v(s)$ was found to be in the interval [2.520, 2.525]). The singular values $\sigma_i[G_v(j\omega)K_v(j\omega)]$ and $\sigma_i[(I+G_v(j\omega)K_v(j\omega)^{-1}]$ of the loop and sensitivity transfer functions are shown in Figs. 11 and 12, respectively. As can be verified from these plots, the frequency domain specifications are met. The loop crossover is approximately at 2 and 1.2 rad/s for the maximum and minimum singular values, respectively, which implies that the settling time should range from approximately 1.5 s up to 2.5 s. The stability margins can be evaluated from the sensitivity singular value plot: in particular, $\|S(s)\|_\infty \approx 3.7$ dB, which implies that $GM\uparrow \geq 9$ dB, $GM\downarrow \leq -8$ dB, and $|PM| \geq 38$ deg.

The poles and zeros of the compensator $K_v(s)$ and closed-loop system $C(s) = [I + G_v(s)K_v(s)]^{-1}\, G_v(s)K_v(s)$ are given in the Appendix.

The resulting output response for the direct lift of 1 deg in θ and γ step command $r_3 = [0\ 1\ 1]^T$ is shown in Fig. 13. Using the same distribution matrix for the pseudocontrol as in the LQG/LTR design, the required control action is shown in Fig. 14. The same comments as in the LQG/LTR design, regarding the discussion of the transients, hold.

Comparison of the LQG/LTR and H_∞ Compensator Designs

From the previous sections, one can conclude that there do not exist any major differences between the two designs. For all practical purposes, the loop shapes are the same, as are the time responses. Furthermore, after the recent developments by Doyle et al.,[14] it is no more difficult to design an H_∞ compensator than it is to design an LQG/LTR one.

More specifically, the H_∞ compensator resulted in slightly better phase and gain margins without any increase in magnitude and speed of the control action. Also, the H_∞ loop shapes were slightly better matched, and the resulting sensitivity transfer function was slightly superior in the low-frequency region. The high-frequency rolloff of the loop in the H_∞ design started at slightly higher frequencies than in the LQG/LTR, which resulted in slightly better stability margins. The

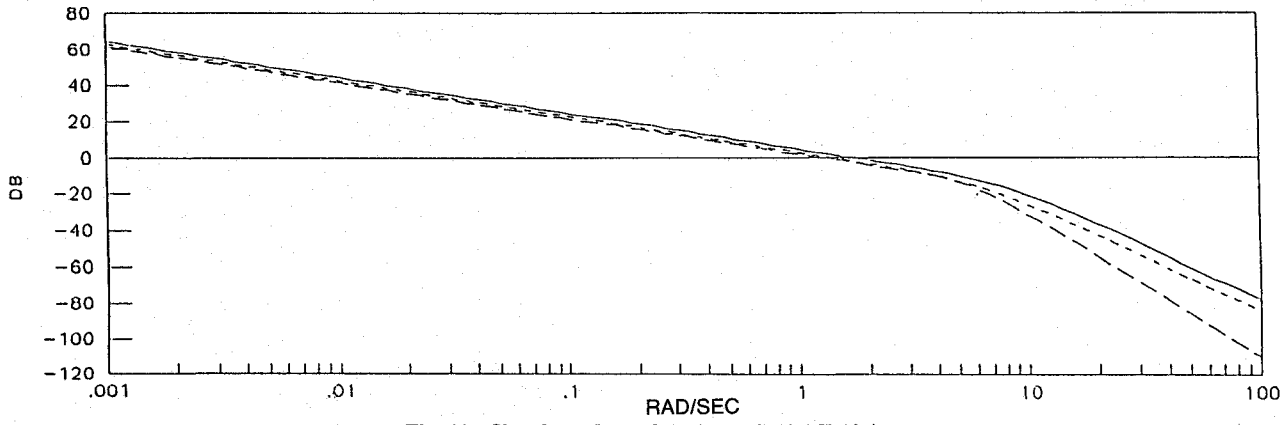

Fig. 11 Singular values of the loop $G_v(j\omega)K_v(j\omega)$.

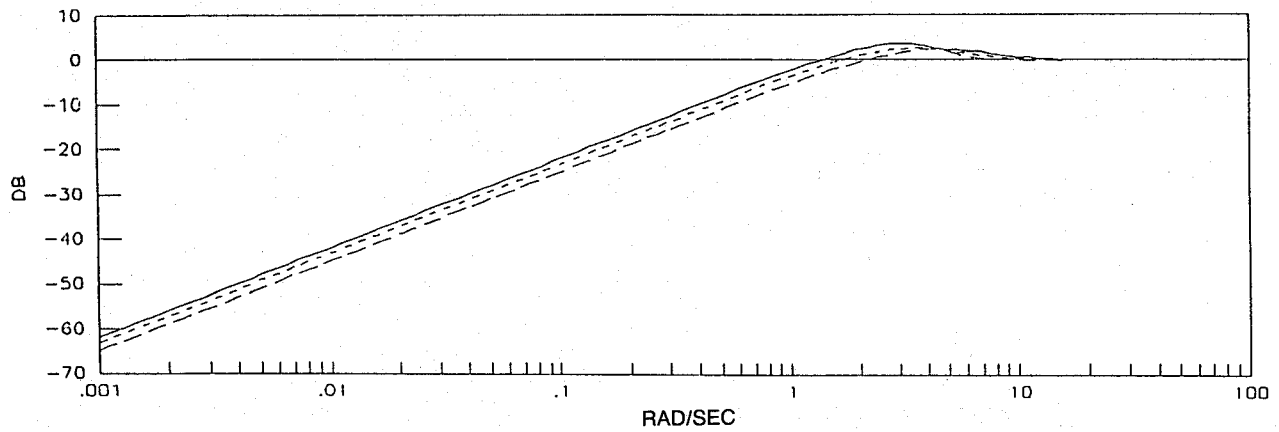

Fig. 12 Singular values of the sensitivity $[I + G_v(j\omega)K_v(j\omega)]^{-1}$.

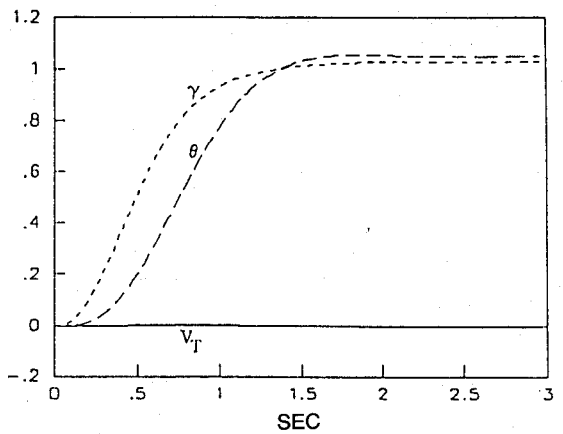

Fig. 13 Output response to r_3.

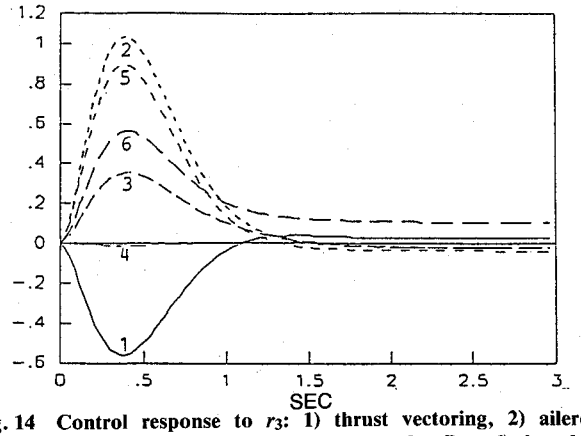

Fig. 14 Control response to r_3: 1) thrust vectoring, 2) aileron, 3) stabilator, 4) leading-edge flap, 5) trailing-edge flap, 6) throttle.

point to make, though, is that these are not significant differences. Moreover, if one takes into consideration that the 13th-order H_∞ compensator has three more states than the 10th-order LQG/LTR compensator, then it becomes very hard to tell which is better. However, in the H_∞ framework, the outputs to be controlled are not required to be measured as they are in the LQG/LTR framework. This fact seems to give an edge to the H_∞ over the LQG/LTR methodology.

Handling of Failures

In the preceding section, LQG/LTR and H_∞ designs were obtained. For each design the final control signals were generated from pseudocontrol signals via a distribution matrix. This was done under the assumption that all actuators were operational. However, this may not be the case. For example, if there is an actuator failure, then the associated control signal cannot be used. In such a situation, if the original distribution algorithm is used, the closed-loop system may go unstable. Instead of redesigning the controller, what we will do is redesign the distribution algorithm. By doing so we not only guarantee nominal stability, but performance remains unaltered. This section addresses the application of the preceding distribution redesign philosophy.

Pseudocontrol Distribution in the Presence of Failures

As already stated the pseudocontrol input v is distributed to the actual control u via the distribution matrix T in such a way so that u^TWu is minimized subject to the constraint $B_1u = v$ where B_1 (known and fixed) $\epsilon R^{3\times 6}$, and $W = W^T > 0$, $W \epsilon R^{6\times 6}$. The resulting T is given by

$$T = W^{-1}B_1^T(B_1W^{-1}B_1^T)^{-1} \tag{13}$$

where, in general, W can have off-diagonal terms. In this paper only diagonal structures of W are considered, i.e., $W = \text{diag}\,(w_1, w_2, w_3, w_4, w_5, w_6)$ with $w_i > 0$, $i = 1, 2, \ldots, 6$.

If the ith control is in fact not usable, then one can simply select $w_i = \infty$ and keep the other weights the same. After performing the minimization with the new weight, call it W_i, a new distribution matrix T_i is obtained. Obviously when this distribution matrix is used, the nominal stability, stability robustness, and performance characteristics of the closed-loop system do not change. This is evident from the fact that the compensator design was based on the pseudosystem $G_\nu(s)$. More specifically the new distribution matrix T_i will be given by

$$T_i = \lim_{w_i \to \infty} W^{-1}B_1^T(B_1W^{-1}B_1^T)^{-1} = \tilde{W}^{-1}\tilde{B}_1^T(\tilde{B}_1\tilde{W}^{-1}\tilde{B}_1^T)^{-1} \tag{14}$$

where $\tilde{W}$ is simply what is left of W if one removes the ith row and column. Analogously, $\tilde{B}_1$ is what is left of B_1 if one were to remove its ith column.

Clearly, the preceding procedure can be generalized if more than one control fails. As expected, this is done by setting the appropriately corresponding weights equal to infinity and performing the minimization. One should note that the number of controls that fail should not exceed three in order for our distribution redesign philosophy to be applicable. This is because, in such a situation, B_1u, where at least four of the elements of u are required to be zero, cannot generate all v in R^3. Hence the constraint $B_1u = v$ cannot, in general, be satisfied when this is the case. Under such extreme conditions, we are forced to redesign the entire control system.

To illustrate the flexibility of the design based on the pseudosystem $G_\nu(s)$, the case of failure of thrust vectoring vane, stabilator, and leading-edge flap was considered. Since the LQG/LTR and H_∞ designs were shown to be virtually identical, we arbitrarily selected the LQG/LTR design. The resulting output response to the 1 deg in θ pitch pointing step command $r_2 = [0\ 0\ 1]^T$ as well as the required control action are shown in Figs. 15 and 16, respectively. As can be noticed, the output tracks the reference with zero steady-state error and with a settling time of 3 s. The controls do not saturate either in magnitude or in rate. A point to make is that in this case there is not any freedom left for different assignment of the controls since the $\tilde{B}_1$ matrix is invertible and therefore $T = \tilde{B}_1$, i.e., the weighting W does not play any role. We should also stress that the output response is identical to the case when all controls are operational.

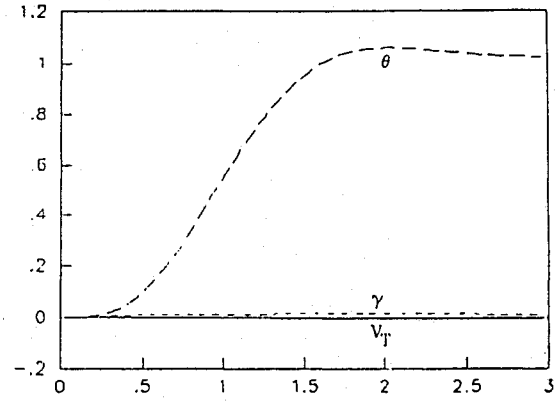

Fig. 15 Output response to r_2 for failed thrust vectoring, stabilator, and leading-edge flap.

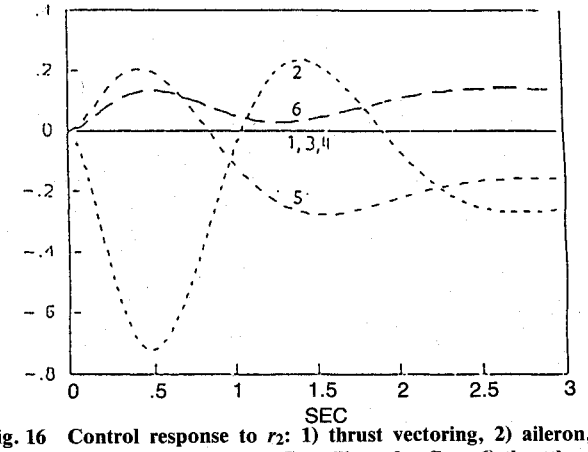

Fig. 16 Control response to r_2: 1) thrust vectoring, 2) aileron, 3) stabilator, 4) leading-edge flap, 5) trailing-edge flap, 6) throttle.

Summary and Conclusions

In this paper, we presented high-performance control-system designs with prescribed robustness margins for the supermaneuverable HARV at a high angle-of-attack ($\alpha = 25$ deg) flight condition where the aircraft is open-loop unstable.

The linear-quadratic-Gaussian/loop-transfer-recovery and H_∞ designs developed in this paper were found to be not very different. In fact, they were virtually identical. Both designs resulted in similar loop shapes and similar compensator strategies. Also, in both designs, the same tradeoffs appear: magnitude saturation limits primarily constrain the bandwidth of the loop, whereas rate saturation limits constrain the stability margins of the system. Although we saw that the H_∞ design obtained is slightly superior, this is counterbalanced by a more complex H_∞ compensator. As with the formal loop shaping linear-quadratic-Gaussian/loop-transfer-recovery design methodology, the H_∞ procedure possesses sufficient degrees of freedom to also address loop shaping (albeit more complicated). However, one advantage of the H_∞ methodology seems to be that it provides a somewhat more general framework since the need for measuring the outputs to be controlled does not exist.

Finally, the technique of pseudocontrol formulation followed in this research offers a great amount of flexibility. This

flexibility is especially useful in cases where certain controls cannot operate due to failures since it utilizes fully the control redundancy. By merely redesigning a distribution matrix from pseudo to actual controls, we not only guarantee nominal stability and stability robustness but performance remains unaltered, i.e., all properties of the pseudosystem are preserved.

Appendix

Numerical Values of A and B Matrices in Eq. (1)

$$A = \begin{bmatrix} -0.0750 & -24.0500 & 0. & -32.1600 \\ -0.0009 & -0.1959 & 0.9896 & 0. \\ -0.0002 & -0.1454 & -0.1677 & 0. \\ 0. & 0. & 1.0000 & 0. \end{bmatrix}$$

$$B = \begin{bmatrix} -0.0230 & 0. & -0.0729 & 0.0393 & -0.0411 & 0.1600 \\ -0.0002 & -0.0001 & -0.0004 & -0.0000 & -0.0003 & -0.0003 \\ -0.0067 & -0.0007 & -0.0120 & -0.0006 & -0.0007 & 0.0005 \\ 0. & 0. & 0. & 0. & 0. & 0. \end{bmatrix}$$

LQG/LTR Design

Poles and zeros of the augmented system, LQG/LTR compensator and closed-loop system.
Poles of $G_a(s)$: $-0.2481 \pm 0.3585j$, $0.0188 \pm 0.1280j$, 0, 0, 0
Zeros of $G_a(s)$: none
Poles of $K_{LQG/LTR}(s)$: $-3.9413 \pm 3.3193j$, $-5.4949 \pm 5.0654j$, $-0.20471 \pm 3.6789j$, -5.2361
Zeros of $K_{LQG/LTR}(s)$: $-0.2481 \pm 0.3585j$, $-0.0178 \pm 0.1244j$
Poles of $C(s)$: $-3.9782 \pm 3.974j$, -2.4364 ± 2.433j, $-1.5752 \pm 2.750j$, $-0.2481 \pm 0.3585j$, $-0.0188 \pm 0.1280j$, -3.1481, -3.0, -3.0, -3.0
Zeros of $C(s)$: $-0.2481 \pm 0.3585j$, $-0.0178 \pm 0.1244j$

H_∞ Design

Poles and zeros of the compensator $K_v(s)$ and closed-loop system $C(s)$.
Poles of $K_v(s)$: $-3.19 \pm 4.59j$, $-5.04 \pm 3.81j$, $-6.17 \pm 5.31j$, -7.75, -1000, -1000, -1000, 0, 0, 0
Zeros of $K_v(s)$: -918.2, -911.7, -916.3, $-0.0180 \pm 0.1248j$, $-0.2481 \pm 0.3585j$, -1000, -1000, -1000
Poles of $C(s)$: -1000, -1000, -1000, $-4.63 \pm 4.05j$, $-2.51 \pm 3.15j$, -6.01, -3.09, -3.05, $-0.2481 \pm 0.3585j$, $-0.0187 \pm 0.1280j$, -3.15, $-3.46 \pm 2.47j$
Zeros of $C(s)$: -911.7, -918.2, -916.3, $-0.0180 \pm 0.1248j$, $-0.2481 \pm 0.3585j$, -1000, -1000, -1000

Acknowledgments

This research was supported by the Air Force Office of Scientific Research, Eglin Air Force Base, under Grant F08635-87- K-0031, by the NASA Ames and Langley Research Centers under Grant NASA/NAG-2-297, and by a gift from the Boeing Corporation.

References

[1]Athans, M., "6.233-6.234 Class Notes," Massachusetts Inst. of Technology, Cambridge, MA, Fall 1987-Spring 1988.

[2]Stein, G., and Athans, M., "The LQG/LTR Procedure for Multivariable Feedback Control Design," *IEEE Transactions on Automatic Control,* Vol. AC-32, No. 2, 1987, pp. 105-114.

[3]Francis, B. A., *A Course in H_∞ Control Theory,* Lecture Notes in Control and Information Sciences, Springer-Verlag, Berlin, 1987.

[4]Lehtomaki, N. A., Sandell, N. R., and Athans, M., "Robustness Results in LQG/LTR Based Multivariable Control Designs," *IEEE Transactions on Automatic Control,* Vol. AC-26, No. 1, 1981, pp.75-93.

[5]Lehtomaki, N. A., "Practical Robustness Measures in Multivariable Control System Analysis," Ph.D. Thesis, Massachusetts Inst. of Technology, Cambridge, MA, LIDS-TH-1093, May 1981.

[6]Doyle, J. C., and Stein, G., "Multivariable Feedback Design: Concepts for a Classical/Modern Synthesis," *IEEE Transactions on Automatic Control,* Vol. AC-26, No. 1, 1981, pp. 4-15.

[7]Safonov, M. G., and Athans, M., "Gain and Phase Margins for Multi-Loop LQG Regulators," *IEEE Transactions on Automatic Control,* Vol. AC-22, No. 2, 1977, pp. 173-179.

[8]Kapasouris, P., "Design for Performance Enhancement in Feedback Control Systems with Multiple Saturating Nonlinearities," Ph.D. Thesis, Dept. of Electrical Engineering, Massachusetts Inst. of Technology, Cambridge, MA, LIDS-TH-1757, March 1988.

[9]Stein, G., "Latest H_∞ Results," unpublished note, Oct. 1987.

[10]Etkin, B., *Dynamics of Flight-Stability and Control,* Wiley, New York, 1982.

[11]Lallman, F. J., "Preliminary Design Study of a Lateral-Directional Control System Using Thrust Vectoring," NASA TM 86425.

[12]Merkel, P., and Whitmoger, R., "Development and Evaluation of Precision Control Modes for Fighter Aircraft," AIAA Guidance and Control Conference, San Diego, CA, 1976.

[13]Voulgaris, P., "High Performance Multivariable Control of the 'Supermaneuverable' F18/HARV Fighter Aircraft," S.M. Thesis, Massachusetts Inst. of Technology, Cambridge, MA, May 1988.

[14]Doyle, J., Glover, K., Khargonekar, P., and Francis, B., "State Space Solutions to Standard H_2 and H_∞ Control Problems," *IEEE Transactions on Automatic Control,* Vol. 34, No. 8, 1989, pp. 831-848.